

Composite Functional Gradient Learning of Generative Adversarial Models

Rie Johnson
RJ Research Consulting
Tarrytown, NY, USA
riejohnson@gmail.com

Tong Zhang
Tencent AI Lab
Shenzhen, China
tzhang@tencent.com

Abstract

Generative adversarial networks (GAN) have become popular for generating data that mimic observations by learning a suitable variable transformation from a random variable. However, empirically, GAN is known to suffer from instability. Also, the theory provided based on the minimax optimization formulation of GAN cannot explain the widely-used practical procedure that uses the so-called $\log d$ trick.

This paper provides a different theoretical foundation for generative adversarial methods which does not rely on the minimax formulation. We show that with a strong discriminator, it is possible to learn a good variable transformation via functional gradient learning, which updates the functional definition of a generator model, instead of updating only the model parameters as in GAN. The theory guarantees that the learned generator improves the KL-divergence between the probability distributions of real data and generated data after each functional gradient step, until the KL-divergence converges to zero. This new point of view leads to enhanced stable procedures for training generative models that can utilize arbitrary learning algorithms. It also gives a new theoretical insight into the original GAN procedure both with and without the $\log d$ trick. Empirical results are shown on image generation to illustrate the effectiveness of our new method.

1 Introduction

We consider observed real data $x_1^*, \dots, x_n^* \in \mathbb{R}^r$ from an unknown distribution p_* on \mathbb{R}^r . Moreover, assume that we are given a random variable Z with a known distribution such as a Gaussian distribution. We are interested in learning a random variable transformation $G(Z)$ so that the generated data $G(Z)$ has a probability density function that is close to the real distribution p_* . This is the setting considered in *generative adversarial networks* (GAN) [6], and the transformation $G(Z)$ is often referred to as a *generator*. While GAN has been widely used, it is also known that GAN is difficult to train due to its instability, which has led to numerous studies, e.g., Wasserstein GAN and its extensions to pursue a different minimax objective [1, 7, 13], mode-regularized GAN to tackle the issue of mode collapse [4], unrolled GAN [12], AdaGAN [19], and references therein.

An important concept introduced by GAN is the idea of *adversarial learner*, denoted here by d , which tries to discriminate real data from generated data. Mathematically, GAN solves the following minimax optimization problem:

$$\max_d \min_G \left[\sum_{x^* \text{ from real data}} \log d(x^*) + \sum_{G(z) \text{ from generated data}} \log(1 - d(G(z))) \right]. \quad (1)$$

Parameterizing d and G , the GAN formulation can be viewed as a saddle point problem in optimization, which can be solved using a stochastic gradient method, where one takes a gradient step with respect to the parameters in d and G (see Algorithm 4 below). However, the practical procedure, suggested by the

original work [6], replaces minimization of $\log(1 - d(G(z)))$ with respect to G in (1) with maximization of $\log(d(G(z)))$ with respect to G , called the *logd trick*. Thus, GAN with the logd trick, though more effective, cannot be directly explained by the theory based on the minimax formulation (1).

This paper provides a new theoretical foundation for generative adversarial methods which does not rely on the minimax formulation (1). We present a theory showing that one can learn a good generator $G(Z)$ where ‘goodness’ is measured by the KL-divergence between the distributions of real data and generated data, by using *functional gradient learning* greedily, similar to gradient boosting [5]. However, unlike the standard gradient boosting, which uses additive models, this paper considers functional compositions in the following form

$$G_t(Z) = G_{t-1}(Z) + \eta_t g_t(G_{t-1}(Z)), \quad (t = 1, \dots, T) \quad (2)$$

to obtain $G(Z) = G_T(Z)$. Here η_t is a small learning rate, and each g_t is a function to be estimated from data. An initial generator $G_0(Z) \in \mathbb{R}^r$ is assumed to be given. We learn from data g_t greedily from $t = 1$ to $t = T$ so that improvement (in terms of the KL-divergence) is guaranteed.

Our theory leads to new enhanced algorithms for learning generative adversarial models that are more stable and effective than GAN. It also provides a new theoretical insight into the original GAN, not only with the minimax formulation but also with the logd trick, thus filling the above-mentioned gap between the theory and the practice of GAN. The experiments show the effectiveness of our new method on image generation in comparison with GAN variants.

Notation Throughout the paper, we use x to denote data in \mathbb{R}^r , and in particular, we use x^* to denote real data. The probability density function of real data is denoted by p_* . We use $\|\cdot\|$ to denote the vector 2-norm and the matrix spectral norm (the largest singular value of a matrix).

2 Functional Gradient Theory of Variable Transformation

To present our theory, we start with stating assumptions (Section 2.1). We then analyze one step of random variable transformation in (2) (i.e., transforming $G_{t-1}(Z)$ to $G_t(Z)$) and examine an algorithm suggested by this analysis (Section 2.2).

2.1 Assumptions

Given weighted training examples $\{(w_i, x_i, \beta_i)\}$ (where $\beta_i \in [0, 1]$ is the probability of binary target y_i such that $P(y_i = 1) = \beta_i$, and $P(y_i = -1) = 1 - \beta_i$), we assume that there is an oracle adversarial learner \mathcal{A} that can solve the following weighted logistic regression problem:

$$\mathcal{A}(\{(w_i, x_i, \beta_i)\}) \approx \arg \min_D \sum_i w_i [\beta_i \ln(1 + \exp(-D(x_i))) + (1 - \beta_i) \ln(1 + \exp(D(x_i)))].$$

Here we use the logistic model, so that d in (1) corresponds to $\frac{1}{1 + \exp(-D(x))}$. In particular, given $\beta \in (0.5, 1]$, real data $x_1^*, \dots, x_n^* \in \mathbb{R}^r$, and generated data $x_1, \dots, x_m \in \mathbb{R}^r$, we let $D(\cdot) = \mathcal{A}(\{(1/n, x_i^*, \beta)\} \cup \{(1/m, x_i, 1 - \beta)\})$, which is often referred to as a *discriminator* that tries to discriminate the real data from the generated data. When n and m are sufficiently large, the standard statistical consistency theory of logistic regression implies that with a strong discriminative learning algorithm \mathcal{A} , we have

$$D(x) \approx \ln \frac{\beta p_*(x) + (1 - \beta)p(x)}{(1 - \beta)p_*(x) + \beta p(x)}, \quad (3)$$

where p_* and p are the probability density functions of real data and generated data, respectively.

For convenience, we impose the following assumption.

Assumption 2.1 *There are constants $c_0, h_0 > 0$ such that when $h \in (0, h_0)$, we have*

$$\begin{aligned} \int \sup_{\|g\| \leq h} |p_*(x) + \nabla p_*(x)^\top g - p_*(x+g)| dx &\leq c_0 h^2, \\ \int \frac{\sup_{\|g\| \leq h} |p_*(x+g) - p_*(x)|^2}{p_*(x)} dx &\leq c_0 h^2, \\ \int \|\nabla p_*(x)\| dx &\leq c_0. \end{aligned}$$

The assumption says that p_* is a smooth density function with light tails. For example, common exponential distributions such as Gaussian distributions and mixtures of Gaussians all satisfy the assumption. It is worth mentioning that the assumption is not truly needed for the algorithm. This is because an arbitrary distribution can always be approximated by mixtures of Gaussians. Nevertheless, the assumption simplifies the statement of our analysis (Theorem 2.1 below) because we do not have to deal with such approximations.

2.2 Analyzing one step of random variable transformation

The goal is to approximate the true density p_* on \mathbb{R}^r through (2). Our analysis here focuses on one step of (2) at time t , namely, random variable transformation of $G_{t-1}(Z)$ to $G_t(Z)$. To simplify notation, we assume that we are given a random variable X with a probability density p on \mathbb{R}^r . We are interested in finding a function $g : \mathbb{R}^r \rightarrow \mathbb{R}^r$, so that the transformed variable $X' = X + \eta g(X)$ for small $\eta > 0$ has a distribution closer to p_* . We show that this can be achieved with a gradient-like step in the function space.

To measure the distance of a density p from the true density p_* , we will keep track of the following KL-divergence

$$L_\beta(p) = \int (\beta p_*(x) + (1-\beta)p(x)) \ln \frac{\beta p_*(x) + (1-\beta)p(x)}{(1-\beta)p_*(x) + \beta p(x)} dx \quad (4)$$

for some $\beta \in (0.5, 1]$, before and after the transformation. We know that $L_\beta(p) \geq 0$ for all p , and $L_\beta(p) = 0$ if and only if $p = p_*$. For $\beta = 1$, $L_\beta(p)$ becomes the standard KL distance between p_* and p .

The following theorem shows that with an appropriately chosen $g(\cdot)$, the transformation $X \rightarrow X + \eta g(X)$ can always reduce the KL-divergence $L_\beta(\cdot)$. This means that transformation $X + \eta g(X)$ is an improvement from X . The proof of the theorem is given in the Appendix A.

Theorem 2.1 *Assume that Assumption 2.1 holds. Let $g : \mathbb{R}^r \rightarrow \mathbb{R}^r$ be a continuously differentiable transformation such that $\|g(\cdot)\| \leq a$ and $\|\nabla g(\cdot)\| \leq b$. Let p be the probability density of a random variable X , and let p' be the probability density of the random variable X' such that $X' = X + \eta g(X)$ where $0 < \eta < \min(1/b, h_0/a)$. For an arbitrary $\beta \in (0.5, 1]$, assume that we have $D_\epsilon(x)$ that is sufficiently close to*

$$\mathcal{D}(x) := \ln \frac{\beta p_*(x) + (1-\beta)p(x)}{(1-\beta)p_*(x) + \beta p(x)}$$

in the sense that it satisfies the ϵ -approximation condition

$$\int p_*(x) \max(1, \|\nabla \ln p_*(x)\|) \left(|D_\epsilon(x) - \mathcal{D}(x)| + \left| e^{D_\epsilon(x)} - e^{\mathcal{D}(x)} \right| \right) dx \leq \epsilon.$$

Further assume that there exists a positive number $B < \infty$ such that $|\mathcal{D}(x)| \leq B$. Then there exists a positive constant c such that for all $\epsilon > 0$:

$$L_\beta(p') \leq L_\beta(p) - \eta \int p_*(x) u(x) g(x)^\top \nabla D_\epsilon(x) dx + c\eta^2 + c\eta\epsilon,$$

where $u(x) = \beta - (1-\beta) \exp(D_\epsilon(x))$.

To see the consequences of the theorem, let us use the strong adversarial learner \mathcal{A} from Section 2.1 to find a discriminator

$$D(\cdot) = \mathcal{A}(\{(1/n, x_i^*, \beta)\} \cup \{(1/m, x_j, 1 - \beta)\}) \quad (5)$$

using real data $\{x_1^*, \dots, x_n^*\}$ and generated data $\{x_1, \dots, x_m\}$, so that (3) holds up to a high accuracy, and therefore $D(x) \approx \mathcal{D}(x)$ (for $\mathcal{D}(x)$ defined in the theorem) to the extent that D satisfies the ϵ -approximation condition for a small $\epsilon > 0$. If we thus use D (as in (5)) as D_ϵ and let $\beta \approx 1$ ¹ and $\epsilon = \eta$ in the theorem, then we have (approximately):

$$L_\beta(p') \leq L_\beta(p) - \eta \int p_*(x) g(x)^\top \nabla D(x) dx + O(\eta^2).$$

If we further take $g(x) = s(x) \nabla D(x)$, where $s(x) > 0$ is a scaling factor, then we have

$$L_\beta(p') \leq L_\beta(p) - \eta \int p_*(x) s(x) \|\nabla D(x)\|_2^2 dx + O(\eta^2). \quad (6)$$

This means that the objective value $L_\beta(\cdot)$ will be reduced for a sufficiently small η unless the following functional gradient vanishes

$$\int p_*(x) s(x) \|\nabla D(x)\|_2^2 dx.$$

The vanishing condition implies that $D(x)$ is approximately a constant when p_* has full support on \mathbb{R}^r . In this case, the discriminator is unable to differentiate the real data from the generated data. Thus, it is implied that letting $g(x) = s(x) \nabla D(x)$ makes the probability density of generated data closer to that of real data until the discriminator becomes unable to distinguish the real data and generated data.

We note that taking $g(x) = s(x) \nabla D(x)$ is analogous to a gradient descent step of $L_\beta(p)$ in the functional space, i.e., a step is taken to modify the function instead of the model parameters. Therefore Theorem 2.1 presents a functional gradient view of variable transformation that *can always improve the quality of the generator* — when the quality is measured by the KL-divergence between the true data and the generated data. As we shall show later, the ability of our theory to use an arbitrary scaling factor $s(x)$ makes it possible to naturally deal with the $\log d$ trick used by GAN practitioners, while the original formulation of GAN in (1) fails to handle the situation.

If we repeat the process described above, the following algorithm is obtained. For simplicity, we only describe the situation with $\beta = 1$; the practical behavior of $\beta \approx 1$ is similar to that of $\beta = 1$. Note that Line 2 was derived by setting $x_j = G_{t-1}(z_j)$ and $\beta = 1$ in (5).

Algorithm 1 CFG: Composite Functional Gradient Learning of Generative Adversarial Nets

Input: real data x_1^*, \dots, x_n^* , initial generator $G_0(z)$ with generated data $\{G_0(z_1), \dots, G_0(z_m)\}$.

Meta-parameter: number of iterations T

- 1: **for** $t = 1, 2, \dots, T$ **do**
 - 2: $D_t(x) \leftarrow \arg \min_D \left[\frac{1}{n} \sum_{i=1}^n \ln(1 + \exp(-D(x_i^*))) + \frac{1}{m} \sum_{i=1}^m \ln(1 + \exp(D(G_{t-1}(z_i))) \right]$
 - 3: $g_t(x) \leftarrow s_t(x) \nabla D_t(x)$ ($s_t(x)$ is for scaling, e.g., most simply $s_t(x) = 1$)
 - 4: $G_t(z) \leftarrow G_{t-1}(z) + \eta_t g_t(G_{t-1}(z))$, for some $\eta_t > 0$.
 - 5: **end for**
 - 6: **return** generator $G_T(z)$
-

We call this algorithm *composite functional gradient learning of GAN (CFG-GAN)*, or simply *CFG*. CFG forms g_t by directly using the functional gradient $\nabla D_t(x)$, as suggested by Theorem 2.1. If (6) holds, and if

¹ Note that in the theorem statement, if we choose $\beta < 1$, then we can take $B = \ln(\beta/(1 - \beta)) < \infty$. However, in practice, one can simply take $\beta = 1$ because the practical behavior of choosing $\beta \approx 1$ is similar to $\beta = 1$.

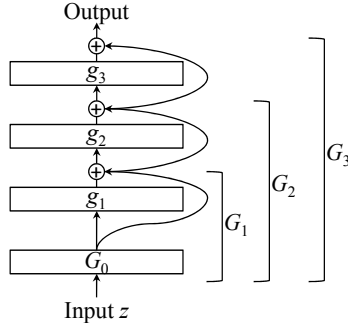


Figure 1: Generator network automatically derived by CFG or ICFG with $T = 3$. ‘ \oplus ’ indicates addition.

we choose $\eta_t = \eta = \epsilon = O(1/\sqrt{T})$, then we can obtain the following bound by cascading (6) from $t = 1$ to $t = T$

$$\frac{1}{T} \sum_{t=1}^T \int p_*(x) s_t(x) \|\nabla D_t(x)\|^2 dx = \frac{1}{T} (O(T\eta) + \eta^{-1} L_\beta(p_0)) = O(T^{-1/2}),$$

where p_0 is the density of $G_0(z)$. This means that as t increases, $\nabla D_t(x) \rightarrow 0$ and thus $D_t(x)$ approaches a constant, assuming p_* has full support on \mathbb{R}^r . That is, in the limit, the discriminator is unable to differentiate the real data from the generated data.

We note that [10] describes a related but different cascading process motivated by Langevin dynamics sampling. Based on the theory of Langevin, repeated noise addition is required in their generation process. Our generation is simpler in that there is no need for noise addition (except for the initial generator). We also provide a theoretical analysis proving the converge of our process to the optimal distribution in the limit.

3 Composite Functional Gradient Algorithms

Starting from the CFG algorithm above, we empirically explored algorithms using image generation as an example task. This section describes variants of CFG that were found to be efficient and effective and discusses their relation to the original GAN.

Notation The algorithms introduced below assume that parametric model definitions (e.g., neural network architectures) are given for use as a discriminator and others (e.g., a generator). When D denotes a discriminator, we write θ_D for the model parameters of D (or θ_G for G). To be terse, we use “discriminator” and “model parameters of the discriminator” interchangeably; e.g., “update the discriminator D ” should be understood as “update the model parameters θ_D of the discriminator D ”.

3.1 ICFG: Incremental composite functional gradient learning

The first change made to CFG is around the discriminator update. CFG (Algorithm 1) optimizes the discriminator to convergence in every iteration. We found on image generation that this tends to cause the discriminator to overfit, and an overfit discriminator is harmful (much more than an underfit one) as it grossly violates the ϵ -approximation condition of our theorem, thus grossly pushing the generator in a wrong direction. We thus considered an incremental variant of CFG, *incremental CFG of GAN (ICFG)*, shown in Algorithm 2. ICFG incrementally updates a discriminator little by little interleaved with the generator updates, so that the generator can keep providing new and more challenging examples to prevent the discriminator from overfitting. That is, similar to GAN, ICFG alternates between a U -minibatch update of the discriminator (where U is a meta-parameter) and one update of the generator.

Algorithm 2 ICFG: Incremental Composite Functional Gradient Learning of Generative Adversarial Nets

Input: a set of training examples S_* , prior p_z , initial generator G_0 , discriminator D at its initial state (e.g., random).

Meta-parameters: number of iterations T . mini-batch size b , discriminator update frequency U .

```
1: for  $t = 1, 2, \dots, T$  do
2:   for  $U$  steps do
3:     Sample  $x_1^*, \dots, x_b^*$  from  $S_*$ , and sample  $z_1, \dots, z_b$  according to  $p_z$ .
4:     Update discriminator  $D$  by descending the stochastic gradient:
           
$$\nabla_{\theta_D} \frac{1}{b} \sum_{i=1}^b [\ln(1 + \exp(-D(x_i^*))) + \ln(1 + \exp(D(G_{t-1}(z_i))))]$$

5:   end for
6:    $g_t(x) \leftarrow s_t(x) \nabla D(x)$  ( $s_t(x)$  is for scaling, e.g., most simply  $s_t(x) = 1$ )
7:    $G_t(z) \leftarrow G_{t-1}(z) + \eta_t g_t(G_{t-1}(z))$ , for some  $\eta_t > 0$ .
8: end for
9: return generator  $G_T$  (and the updated discriminator  $D$  if so desired).
```

ICFG shares nice properties with CFG, in contrast to GAN. First, the generator is guaranteed to improve with each update to the extent that the assumptions hold; therefore, it is expected to be stable. Second, there is no need to design a complex generator model. In a sense, the generator model is automatically and implicitly derived from the discriminator, and it dynamically *grows* as training proceeds. Figure 1 illustrates a generator created by ICFG with $T = 3$ (i.e., 3 iterations). As is clear from the illustration, the generator forms a *residual net* [8], where each building block g_t is automatically derived from the discriminator at time t .

A shortcoming, however, is that the implicit generator network can become very large. At time t , the size of the generator network is in $O(t)$, and therefore, the cost for computing $G_t(z)$ starting from scratch is in $O(t)$. This means that the computational cost for performing T iterations of training could be in $O(\sum_{t=1}^T t) = O(T^2)$. Therefore, on a task that requires many iterations (i.e., a large T), training would become quite expensive. We found that image generation requires a relatively large T , e.g., $T > 1000$, and that T in this order is problematic, causing slow training, a large model that takes up a lot of space, and slow image generation.

A partial remedy, which speeds up training (but not generation), is to have an *input pool* of a finite size. That is, we restrict the input distribution to be on a finite set S_z and for every input $z \in S_z$, maintain $G_{t'}(z)$ for the latest t' for which $G_{t'}(z)$ was computed. By doing so, when $G_t(z)$ needs to be computed, one can start from $G_{t'}(z)$ instead of starting over from $G_0(z)$, which saves computation time. With an input pool S_z of an extremely small size, $G_{t-1}(z)$ would be available for any $z \in S_z$ whenever $G_t(z)$ is required; in that case, $G_t(z)$ can be obtained for any z in $O(1)$, which makes the cost of training with T iterations be in $O(T)$ instead of $O(T^2)$. Therefore, the order of ICFG training with a finite input pool is in $O(T^q)$ for $1 \leq q < 2$. However, a very small input pool should be avoided as it would fail to provide a variety of examples to the discriminator; also, this remedy solves only a part of the problem.

3.2 xICFG: Approximate incremental composite functional gradient learning

As a complete solution to the issue of large generators, we propose *Approximate ICFG* (*xICFG*, Algorithm 3). xICFG periodically compresses the generator obtained by ICFG, by training an *approximator* of a fixed size that approximates the behavior of the generator obtained by ICFG. That is, given a definition of an approximator \tilde{G} and its initial state, xICFG repeatedly alternates the following.

- Using the approximator \tilde{G} as the initial generator, perform T iterations of ICFG to obtain generator G .
- Update the approximator \tilde{G} to achieve $\tilde{G}(z) \approx G(z)$.

The generator size is again in $O(T)$, but unlike ICFG, which requires T to be large (e.g., $T > 1000$) for complex tasks such as image generation, xICFG can keep T small (e.g., $T = 10$), thus xICFG is efficient. We

Algorithm 3 xICFG: Approximate Incremental Composite Functional Gradient Learning of GAN

Input: a set of training examples S_* , prior p_z , approximator \tilde{G} at its initial state, discriminator D .

Meta-parameters: input pool size, meta-parameters (T, b, U) for ICFG.

- 1: **loop**
 - 2: $S_z \leftarrow$ an input pool of the given size, sampled according to p_z .
 - 3: $q_z \leftarrow$ the uniform distribution over S_z .
 - 4: $G, D \leftarrow$ output of ICFG using S_*, q_z, \tilde{G}, D as input.
 - 5: **if** some exit criteria are met **then**
 - 6: **return** generator G
 - 7: **end if**
 - 8: Update the approximator \tilde{G} to minimize $\sum_{z \in S_z} \frac{1}{2} \|\tilde{G}(z) - G(z)\|^2$
 - 9: **end loop**
-

use the idea of an input pool above for speeding up training, and instead of keeping the same pool to the end, we refresh the pool S_z in every iteration of xICFG (Lines 2&3 of Algorithm 3). For speed, the values $G_{t'}(z)$ for $z \in S_z$ for the latest t' should be kept not only for use in ICFG but also for preparing the training data $\{(z, G(z)) \mid z \in S_z\}$ for the training of the approximator \tilde{G} (Line 8). Doing so, the runtime of one iteration of xICFG is in $O(|S_z| |\theta_D| T + |S_z| |\theta_{\tilde{G}}|)$, where $|S_z|$ is the input pool size, and $|\theta_D|$ and $|\theta_{\tilde{G}}|$ represent the model sizes of the discriminator and the approximator, respectively. Both a small pool size $|S_z|$ and a small T would reduce the runtime of one iteration, but they would increase the number of required iterations, as they reduce the amount of the improvement achieved by one iteration of xICFG, and so a trade-off should be found empirically. In particular, approximation typically causes some degradation, and so it is important to set T and $|S_z|$ to sufficiently large values so that the amount of the generator improvement exceeds the amount of degradation caused by approximation. In our experiments, however, tuning of meta-parameters turned out to be relatively easy; one set of meta-parameters achieved stable training in all the tested settings across datasets and network architectures, as shown later.

3.3 Relation to GAN

GAN has been shown to be effective on the image generation tasks, but it is also known that training of GAN can be hard due to its instability. In this section, we show that GAN (Algorithm 4) can be regarded as a coarse approximation of ICFG, and it is closely related to a special case of xICFG that sets the meta-parameters to extreme values. This viewpoint leads to some insight into GAN's instability.

We start with the fact that *GAN and ICFG share the discriminator update procedure*. This fact becomes

Algorithm 4 GAN: Generative Adversarial Networks [6]

Input: a set of training examples S_* , prior p_z , discriminator d such that $d(\cdot) \in [0, 1]$, generator G .

Meta-parameters: mini-batch size b , discriminator update frequency U .

- 1: **repeat**
 - 2: **for** U steps **do**
 - 3: Sample x_1^*, \dots, x_b^* from S_* , and sample z_1, \dots, z_b according to p_z .
 - 4: Update discriminator d by ascending the stochastic gradient:
$$\nabla_{\theta_d} \frac{1}{b} \sum_{i=1}^b [\ln d(x_i^*) + \ln(1 - d(G(z_i)))]$$
 - 5: **end for**
 - 6: Sample z_1, \dots, z_b according to p_z .
 - 7: Update the generator by descending the stochastic gradient: $\nabla_{\theta_G} \frac{1}{b} \sum_{i=1}^b \ln(1 - d(G(z_i)))$
 - 8: **until** some exit criteria are met
 - 9: **return** generator G
-

more obvious, when we note that the last step of the GAN discriminator d is typically the sigmoid function to make probability estimates using the logistic model, and so let us write $d(x) = \frac{1}{1+\exp(-D(x))}$. By plugging it into $\nabla_{\theta_d} \frac{1}{b} \sum_{i=1}^b [\ln(d(x_i^*)) + \ln(1 - d(G(z_i)))]$, which is for GAN discriminator update (Line 4 of Algorithm 4), to rewrite it in terms of D , we obtain exactly the same gradient used for ICFG discriminator update (Line 4 of Algorithm 2) by flipping the sign and ‘descend’/‘ascend’. Thus, ICFG shares discriminator update with GAN, provided that the last step of GAN’s discriminator is the sigmoid.

Next, we show that *the generator update of GAN is equivalent to coarsely approximating a generator produced by ICFG*; in more detail, it is equivalent to taking one step of gradient descent in order to approximate the generator produced by ICFG with $T = 1$. To see this, first note that GAN’s generator update (Line 7 of Algorithm 4) requires the gradient $\nabla_{\theta_G} \ln(1 - d(G(z)))$. Using $d(x) = \frac{1}{1+\exp(-D(x))}$ again, and writing $[v]_i$ for the i -th component of vector v , the k -th component of this gradient can be written in terms of D as:

$$[\nabla_{\theta_G} \ln(1 - d(G(z)))]_k = \left[\nabla_{\theta_G} \ln \frac{\exp(-D(G(z)))}{1 + \exp(-D(G(z)))} \right]_k = -s_0(G(z)) \sum_j [\nabla D(G(z))]_j \frac{\partial [G(z)]_j}{\partial [\theta_G]_k} \quad (7)$$

where $s_0(x) = \frac{1}{1+\exp(-D(x))}$, a scalar resulting from differentiating $f(y) = -\ln \frac{\exp(-y)}{1+\exp(-y)}$ at $y = D(x)$. Now suppose that we apply ICFG with $T = 1$ to a generator G to obtain a new generator G' :

$$G'(z) = G(z) + \eta g(G(z)) = G(z) + \eta s(G(z)) \nabla D(G(z)) ,$$

and then we update G to approximate G' so that

$$\frac{1}{2} \|G'(z) - G(z)\|^2$$

is minimized as in xICFG. To take one step of gradient descent for this approximation, we need the gradient of the square error above with respect to θ_G . It is easy to verify that the k -th component of this gradient is:

$$\left[\nabla_{\theta_G} \frac{1}{2} \|G'(z) - G(z)\|^2 \right]_k = - \sum_j [G'(z) - G(z)]_j \frac{\partial [G(z)]_j}{\partial [\theta_G]_k} = -\eta s(G(z)) \sum_j [\nabla D(G(z))]_j \frac{\partial [G(z)]_j}{\partial [\theta_G]_k} .$$

By setting the scaling factor $s(x) = s_0(x)/\eta$, this is exactly the same as (7) for GAN’s generator update. (Recall that our theory and algorithms accommodate an arbitrary data-dependent scaling factor $s(x) > 0$.)

Thus, algorithmically GAN can be viewed as a modification² of a special case of xICFG that does the following:

- Set $T = 1$, i.e., let ICFG update the generator *just once*.
- To update the approximator, take *only one* gradient descent step with *only one* mini-batch, instead of optimizing to the convergence with many examples. Therefore, the degree of approximation could be poor.

The same argument applies also to the $\log d$ -trick variant of GAN. The generator update with the $\log d$ trick requires the same gradient as (7) except that s_0 becomes $s_1(x) = \frac{1}{1+\exp(D(x))}$; note that the change from $s_0(x) = \frac{1}{1+\exp(-D(x))}$ is the sign in front of D . Thus, GAN with the $\log d$ trick can also be viewed as a modification of a special case of xICFG above.

Moreover, to compare GAN with and without the $\log d$ trick, consider the situation where generated data x is very far from the real data and therefore $D(x) \ll 0$. In this situation, we have $s_0(x) \approx 0$ without the $\log d$ trick, which would make the gradient (for updating θ_G) vanish, as noted in [6], even though the generator is poor and so requires updating. In contrast, we have $s_1(x) \approx 1$ with the $\log d$ trick in this poor generator situation, and when the generated data x is close to the real data and therefore $D(x) \approx 0$, we have $s_1(x) \approx \frac{1}{2}$.

² Although GAN is closely related to a special case of xICFG, there are differences. For example, GAN uses no input pool; GAN returns the approximator while xICFG returns the generator created by ICFG.

Thus, with the $\log d$ trick, the scaling factor of the gradient is likely to fall into $[\frac{1}{2}, 1)$, which is more sensible as well as more similar to our choice ($s(x) = 1$) for the xICFG experiments, compared with the scaling of GAN without the trick.

GAN is known to be unstable while xICFG with appropriate meta-parameters is stable, as shown later. Thus, we figure that GAN’s instability derives from their algorithmic differences, the two bullets above – an extremely small T and coarse approximation, both of which can cause degradation of the generator. When this happens, a GAN generator could fail to keep providing challenging examples to the discriminator, which would disrupt the balance of the progress of the discriminator and that of the generator, leading to instability.

Finally, note that a fundamental theoretical difference between our CFG algorithms and GAN lies in the optimization objectives. With the optimal discriminator, the objective of GAN in its original form (without the $\log d$ trick) can be regarded as minimization of the Jensen-Shanon (JS) divergence between the distributions of real data and generated data [6]:

$$\int p_*(x) \ln \frac{2p_*(x)}{p_*(x) + p(x)} dx + \int p(x) \ln \frac{2p(x)}{p_*(x) + p(x)} dx.$$

By contrast, Theorem 2.1 implies that CFG and its variants directly minimize the KL-divergence between the distributions of real data and generated data defined in (4). Since minimizing the KL-divergence is equivalent to maximizing the log-likelihood, CFG is similar to a maximum likelihood estimate. Therefore, we expect that our methods can be more easily combined with other maximum likelihood based probability models. More generally, the idea of composite functional gradient is similar to gradient descent, but the descent step is taken in the functional space instead of the model parameter space. In its original form, the complexity of the generator grows as the iteration proceeds. It can be shown that this approach also simultaneously minimizes some other distance functions such as JS divergence. The ability to optimize multiple criteria simultaneously may be one reason why CFG-based procedures (including its variants) are stable.

4 Experiments

We tested xICFG on the image generation task.

4.1 Experimental setup

4.1.1 Baseline methods

Due to its relation to xICFG as analyzed above, we also experimented with the original GAN for comparison. More specifically, we tested two types of the original GAN as proposed in [6], which we call GAN0 and GAN1 below when they need to be distinguished:

- GAN0: GAN *without* the $\log d$ trick. [6] provided a theoretical analysis of GAN0.
- GAN1: GAN *with* the $\log d$ trick. GAN1 was suggested by [6] for practical use.

As a representative of state-of-the-art methods, we tested Wasserstein GAN with the gradient penalty proposed in [7] (hereafter, ‘WGANgp’). Different from GAN, the training objective of WGAN is

$$\min_{\theta_G} \max_{\theta_D} [\mathbb{E}_{x^* \sim p_*} D(x^*) - \mathbb{E}_{z \sim p_z} D(G(z))] .$$

WGAN was proposed by [1] and shown to achieve stable training with meaningful discriminator³ output values. However, weight clipping used in [1] for enforcing a Lipschitz constraint on the discriminator was found to cause training failure [7, 13]. WGANgp enforces a Lipschitz constraint through a *gradient penalty* term $\sum_i (\|\nabla D(\epsilon x_i^* + (1 - \epsilon)x_i)\| - 1)^2$ where $\epsilon \sim U[0, 1]$ and x_i^* and x_i are sampled from real data and generated data, respectively. It has been shown to achieve stable training on a number of network architectures and

³ A discriminator is called ‘critic’ in WGAN studies, but we call it ‘discriminator’ to be consistent with other methods.

datasets. We consider WGANgp to represent the state of the art as it was shown to rival or outperform a number of previous methods such as the original WGAN with weight clipping, Least Squares GAN [11], Boundary Equilibrium GAN [3], GAN with denoising feature matching [20], and Fisher GAN [13].

4.1.2 Evaluation metrics

Making reliable likelihood estimates with generative adversarial models [17] is known to be challenging, and we instead focused on evaluating the visual quality of generated images, using datasets that come with labels for classification. We measured the *inception score* [16]. The intuition behind this score is that high-quality images should lead to high confidence in classification. It is defined as $\exp(\mathbb{E}_x \text{KL}(p(y|x)||p(y)))$ where $p(y|x)$ is the label distribution conditioned on generated data x and $p(y)$ is the label distribution over the generated data. Following previous work (e.g., [21, 4]) the probabilities were estimated by a classifier trained with labels for the classification task (instead of the ImageNet-trained inception model used in [16]) so that the image classes of interest were well represented in the classifier. To evaluate the diversity of generated images, we also measured the KL-divergence between the distributions of predicted labels over generated data and true labels over the real data, as suggested by [4]. However, we found that in our settings, this measure correlates to the inception score, and so we do not report it to avoid redundancy. We note that the inception score is limited, e.g., it would not detect mode collapse or missing modes within a class. Apart from that, we found that the inception score corresponds to human perception well. The only exceptions occasionally observed were when the images were of very low quality, e.g., at the beginning of training.

4.1.3 Data

We used MNIST, the Street View House Numbers dataset (SVHN) [14], and the large-scale scene understanding (LSUN) dataset⁴. These datasets are provided with class labels (digits ‘0’ – ‘9’ for MNIST and SVHN and scene types for LSUN). On each dataset, we used the images in the training set as the training examples of real data. There are 10 classes in LSUN, and a number of studies have used the images of only one class (‘bedroom’) for image generation. However, since a single-class dataset would preclude objective evaluation using class labels (described above), we instead generated a balanced two-class dataset by using the same number of training images from the ‘bedroom’ class and the ‘living room’ class (LSUN BR+LR). Similarly, we generated a balanced dataset from the ‘tower’ class and the ‘bridge’ class (LSUN Tower+Bridge). The number of the images used as the training examples was 60K (MNIST), 521K (SVHN, the ‘extra’ set minus 10K for validation), 2.6 million (LSUN BR+LR), and 1.4 million (LSUN Tower+Bridge). MNIST is 1-channel 28×28 , and SVHN is 3-channel 32×32 . The LSUN images (3-channel) were shrunk and cropped into 64×64 from the original rectangle images, following [15, 1]. No preprocessing was applied except that the pixel values were scaled into $[-1, 1]$.

The inception scores of the real data (measured on a set of 10K real images for validation, disjoint from the training set) were 9.91 (MNIST), 9.13 (SVHN), 1.84 (LSUN BR+LR), and 1.90 (LSUN Tower+Bridge), respectively, which roughly set the upper bounds of the score that can be achieved by generated images.

4.1.4 Network architectures

The tested methods require as input a network architecture of a discriminator and that of an approximator or a generator. While there are numerous network architectures we could experiment with, we focused on two types of architecture pairs with two distinct merits – good results and simplicity.

The first type is with complexity appropriate for the dataset, so that relatively good results can be obtained. On MNIST and SVHN, we used an extension of DCGAN [15]. The DCGAN discriminator consists of convolution layers with stride 2 and batch normalization, and the generator is essentially the reverse of the discriminator, using transposed convolution layers with stride 2 and batch normalization. Our extension is mainly to add 1×1 convolution layers, which improved the results without much increase of computational cost. Larger (64×64) images of LSUN were found to benefit from more complex networks, and so we used a

⁴ <http://lsun.cs.princeton.edu/2015.html>

b	mini-batch size	64
$ S_z $	input pool set size	$10b$
U	discriminator update frequency	1
T	number of iterations in ICFG	25

Table 1: Meta-parameters used in the xICFG experiments. For simplicity, these meta-parameters were fixed irrespective of datasets or network architectures. An exception is Section 4.2.3 where we seek smaller T 's for the advantages of smaller generators.

residual net (ResNet) [8] of four residual blocks, which we adopted from the WGANgp code release, for both the discriminator and the approximator/generator. Detailed definitions are given in Appendix B.

All of these networks include batch normalization layers. As noted in the original work [7], WGANgp does not work well with a discriminator with batch normalization (essentially, scaling by batch normalization interferes with implicit scaling via the gradient penalty), while the other tested methods typically benefit from batch normalization. Although it would be ideal to use exactly the same network architectures for all the methods, it would be rather unfair for the other methods if we always remove batch normalization. Therefore, we do the following. For each combination of network definitions and datasets, we test WGANgp with the following three options, (1) replacing batch normalization in the discriminator with layer normalization [2], (2) removing batch normalization only from the discriminator, and (3) removing batch normalization from both the discriminator and the generator, and report the best results, while the other methods use the network definitions as they are. In addition, we test the setting where no batch normalization is used in either discriminators or approximators/generators.

The second type of network architecture we tested uses a minimally simple approximator/generator, consisting of two 512-dim fully-connected layers with ReLU, followed by the output layer with tanh, which has a merit of simplicity, requiring less design effort. We combined it with a convolutional discriminator, the DCGAN extension above.

4.1.5 xICFG implementation details

The pixel values of images need to be in a certain range. The approximator network makes them in range by tanh, but addition of $\eta_t g_t$ in ICFG can make the values go out of range. To avoid out-of-range pixel values, a truncation step was added to ICFG after the addition of $\eta_t g_t$. To speed up training, we limited the number of epochs of the approximator training in xICFG to 10 while reducing the learning rate by multiplying 0.1 whenever the training loss stops going down. The scaling function $s(x)$ in ICFG was set to $s(x) = 1$. To initialize the approximator \tilde{G} for xICFG, we first created a simple generator $G_{\text{rand}}(z)$ equipped with a projection layer with random weights set by the Gaussian distribution with zero mean and standard deviation 0.01 (to produce data points of the desired dimensionality), followed by tanh, and then trained \tilde{G} to approximate the behavior of G_{rand} . The training time reported below includes the time spent for this initialization.

4.1.6 Other details

In all cases, the prior p_z was set to generate 100-dimensional normally distributed vectors with zero mean and standard deviation 1: $\mathcal{N}(\mathbf{0}, \mathbf{I})$.

Table 1 shows the meta-parameter values used for obtaining the xICFG results reported below. They were simply fixed for all the xICFG experiments. An exception is Section 4.2.3 where we pursue smaller T 's for practical advantages. For GAN, we used the same mini-batch size as xICFG, but we set the discriminator update frequency U to 1 as other values led to poorer results.

The SGD update was done with *rmsprop* [18] for xICFG and GAN (i.e., GAN0 and GAN1). The learning rate for rmsprop was simply fixed to 0.0001 for xICFG, but we tried several values for GAN as it turned out to be critical. Similarly, for xICFG, we found it important to set the step size η for the generator update in ICFG to an appropriate value. Therefore, we tried several values for these two meta-parameters (one for

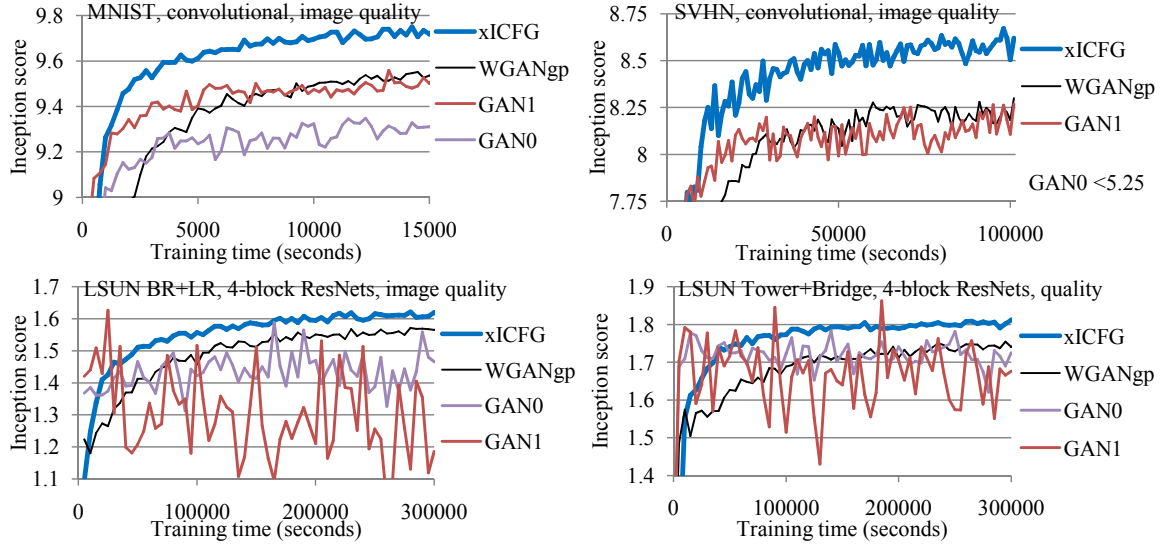


Figure 2: Image quality. Convolutional networks. The legends are sorted from the best to the worst. xICFG outperforms the others.

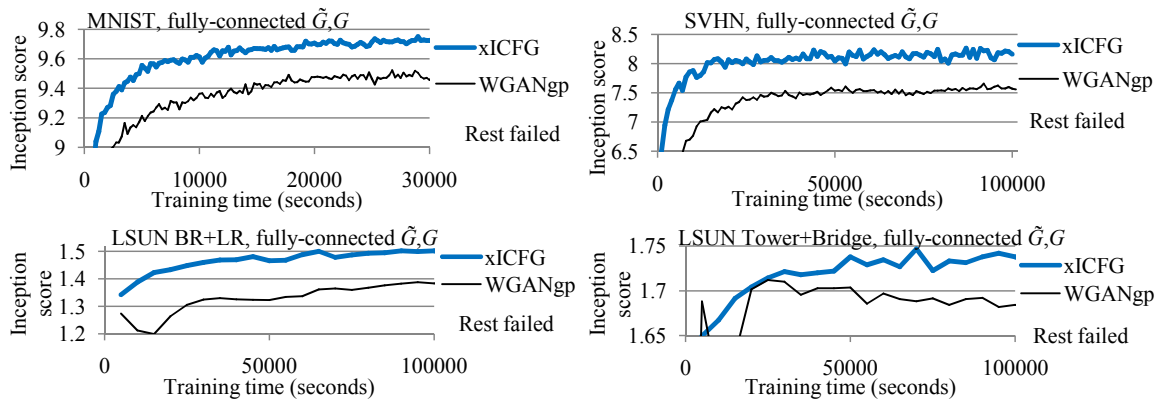


Figure 3: Image quality. Fully-connected approximators/generators. xICFG outperforms the others.

xICFG and one for GAN) with the following protocol. We chose the values based on the inception score on the validation set of 10K input vectors (i.e., 10K 100-dim Gaussian vectors), and then we used the chosen values to measure the inception scores on the test set of 10K input vectors, disjoint from the validation set.

The SGD update for WGANgp was done with the Adam optimizer [9] as it was used in the original study [7]. We set all the meta-parameters for WGANgp to the values suggested by the original study (which we also confirmed to be nearly the optimum), except that we tried several values for α (learning rate for Adam), as it turned out to be critical.

Thus, the amount of meta-parameter tuning effort was about the same for all the tested methods except for WGANgp, which required additional search for the normalization options.

All the experiments were done using a single NVIDIA Tesla P100.

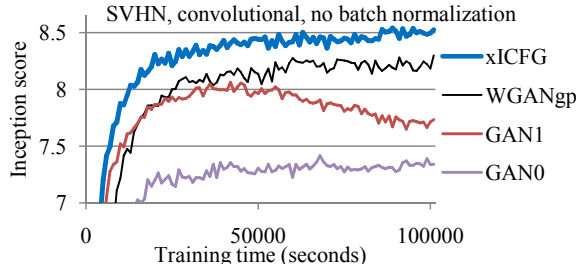


Figure 4: No batch normalization anywhere. Convolutional networks. SVHN. The legends are sorted from the best to the worst. xICFG outperforms the others.

4.2 Results

4.2.1 On the quality of generated images

First, we report the inception score results, indicative of the quality of generated images, on the convolutional networks (aiming at good results) in Figure 2. The x -axis represents time spent for training. xICFG generally outperforms the others on all the datasets. Although on LSUN datasets GAN0 and GAN1 occasionally appear to rival or exceed xICFG, inspection of generated images reveals that they both suffer from mode collapse. The inception score results with the simple but weak (fully-connected) approximator/generator are shown in Figure 3. xICFG again outperforms the others on all the datasets. Among the baseline methods, WGANgp is the only one method that succeeded with the weak generator, but its inception score fell short behind xICFG. In addition, Figure 4 shows the inception score results on the convolutional networks without batch normalization anywhere. xICFG outperforms the others. These results show that xICFG is effective and efficient.

Examples of generated images are shown in Figures 5–8. On MNIST (Figure 5), all the generated images seem to be of relatively high-quality except for (g) the worst baseline with the fully-connected (f.c.) generator. However, looking closely, one may notice that those with lower scores (numbers in the parentheses) include a few more images of slightly lower quality (i.e., harder to tell what digits they are). The quality differences between methods are more obvious on SVHN (Figure 6); in particular, with the simple fully-connected generator, xICFG generates decent images shown in (e), while the images generated by the best baseline in (f) are less sharp and the worst baseline in (g) suffers from severe mode collapse. On LSUN BR+LR (Figure 7), with the convolutional networks (b-d), the images generated by xICFG appear to be at least as good as the images by the best baseline, WGANgp, which is the state of the art. The second best baseline, GAN0, suffers from low quality and lack of diversity. When the fully-connected approximator or generator is used, xICFG generates clearly higher-quality images than the other tested methods (compare (e) with (f) and (g) of Figure 7). We see the similar trends on LSUN Tower+Bridge (Figure 8), where the advantage of xICFG is even more prominent. More examples of LSUN images are shown in Figures 13 and 14.

When generated images look somewhat realistic, one may wonder if the generator is memorizing training images instead of capturing the essence of images. In Figure 9, we show examples that indicate that xICFG does something more ‘creative’ than memorization. The LSUN Tower+Bridge includes a number of pictures of Golden Gate Bridge. As seen in Figure 9a, in reality, Golden Gate Bridge’s tower component (the reddish vertical object) has four grids above the horizontal part. xICFG generates images that look like Golden Gate Bridge (Figure 9b) though they are not perfect (the towers look good, but the wires are wobbly and the ocean is missing from some). It also generates images that look like modifications of Golden Gate Bridge (Figure 9c), making the tower component longer with more grids, placing it with objects that are not there in reality, and so forth.

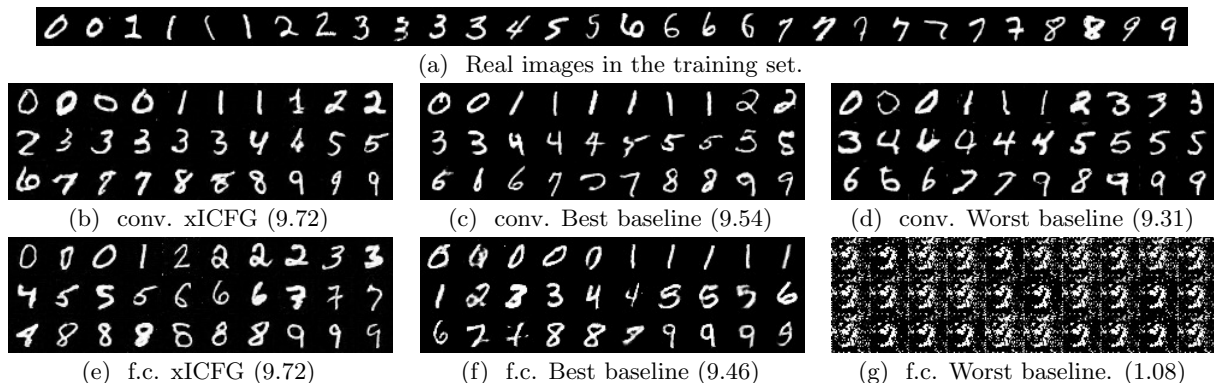


Figure 5: MNIST. (a) Real images from the training set. (b-d) Generated images after 15K seconds of training with convolutional networks (Fig 2). (e-g) Generated images after 30K seconds of training with fully-connected approximators/generators (Fig 3). Randomly chosen and sorted by the predicted classes. The numbers in the parentheses are the inception scores averaged over 10K images.

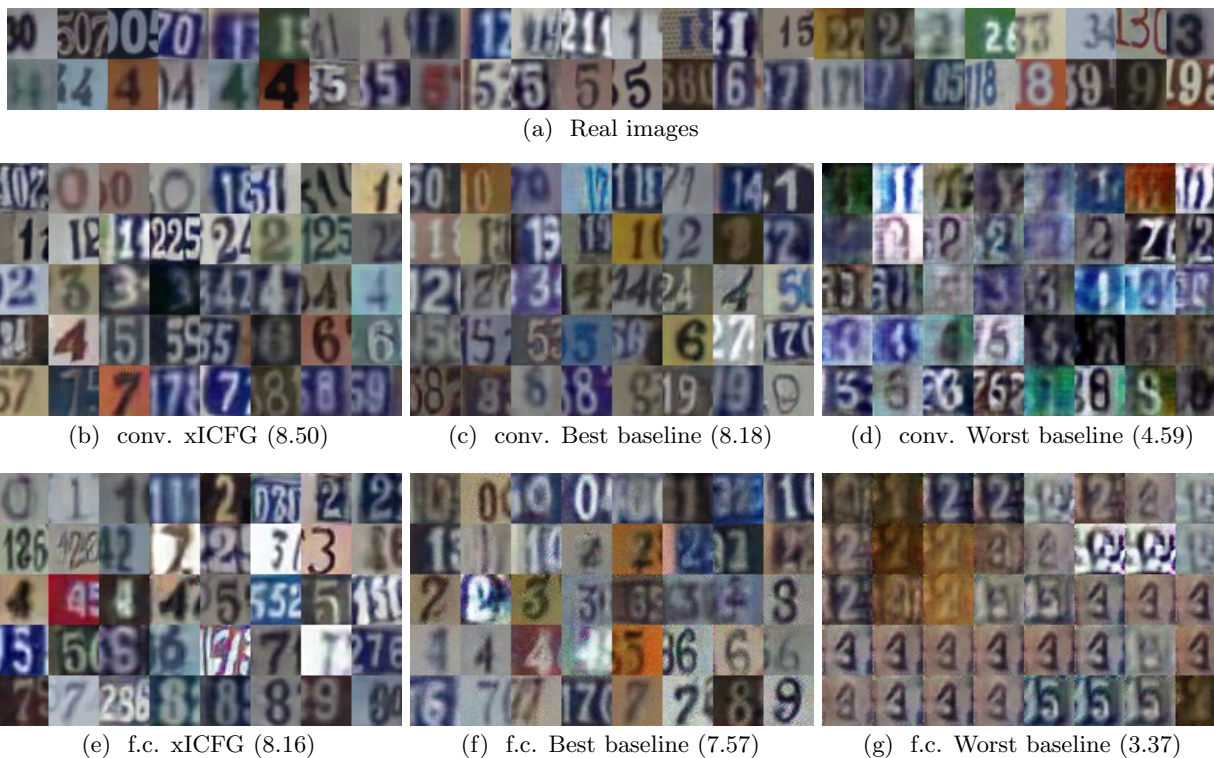
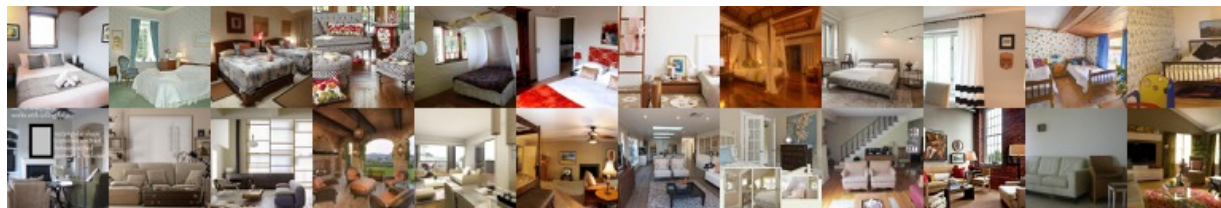


Figure 6: SVHN. (a) Real images in the training set. (b-g) Images generated after 100 K seconds of training. With the convolutional generator/approximator as in Fig 2 (b-d), and with the fully-connected generator/approximator as in Fig 3 (e-g). The images were randomly chosen and sorted by the predicted classes ('0'-'9'). The numbers in the parentheses are the inception scores averaged over 10K images.



(a) Real images



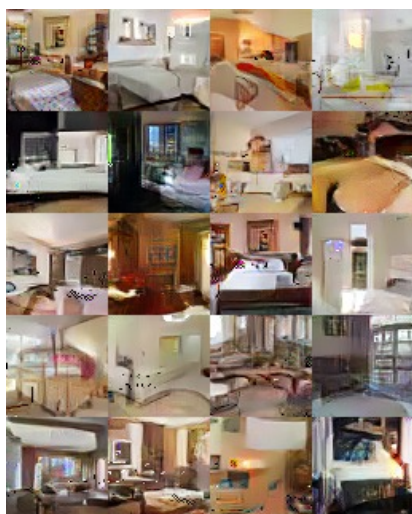
(b) conv. xICFG (1.62)



(c) conv. Best baseline (1.57)



(d) conv. 2nd best baseline (1.47)



(e) f.c. xICFG (1.50)



(f) f.c. Best baseline (1.38)



(g) f.c. 2nd best baseline (1.12)

Figure 7: LSUN bedrooms and living rooms (64×64). (a) Real images in the training set. (b-d) Images generated after 300K seconds of training with 4-block ResNets as in Fig 2. (e-g) Images generated after 100K seconds of training with a fully-connected approximator/generator as in Fig 3. The images were randomly chosen and sorted by the predicted classes. The numbers in the parentheses are the inception scores averaged over 10K images.



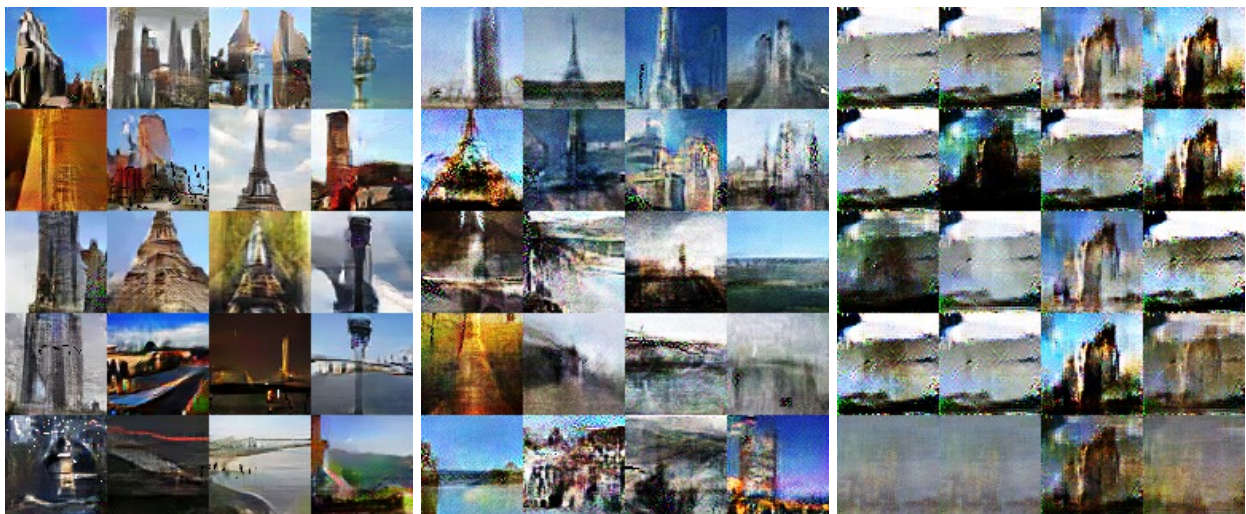
(a) Real images



(b) conv. xICFG (1.81)

(c) conv. Best baseline (1.75)

(d) conv. 2nd best baseline (1.72)



(e) f.c. xICFG (1.74)

(f) f.c. Best baseline (1.68)

(g) f.c. 2nd best baseline (1.58)

Figure 8: LSUN towers and bridges (64×64). (a) Real images in the training set. (b-d) Images generated after 300K seconds of training with 4-block ResNets as in Fig 2. (e-g) Images generated after 100K seconds of training with a fully-connected approximator/generator as in Fig 3. The images were randomly chosen and sorted by the predicted classes. The numbers in the parentheses are the inception scores averaged over 10K images.



Figure 9: “Realistic” and “creative” images generated by xICFG. (a) Real Golden Gate Bridge images in the training set. (b) Images generated by xICFG that look like Golden Gate Bridge though not perfect. (c) Images generated by xICFG that look like modifications of Golden Gate Bridge.

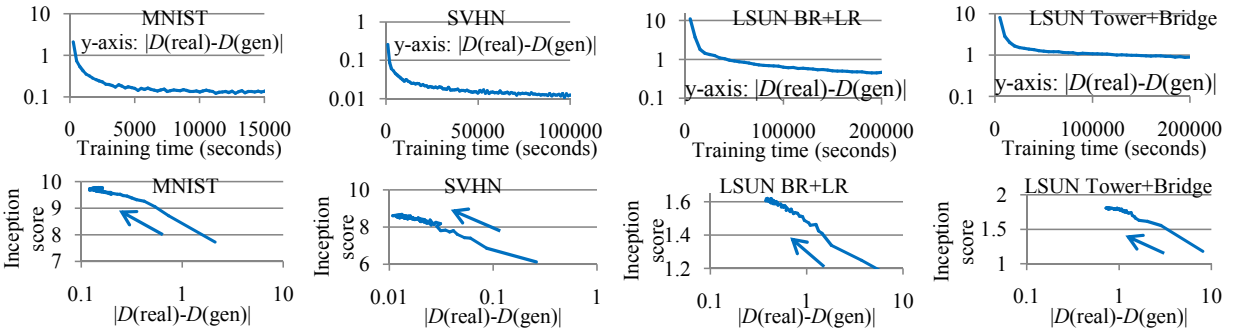


Figure 10: $|D(\text{real})-D(\text{gen})|$ and its relation to image quality. xICFG. On the runs in Figure 2. The arrows in the lower row indicates the direction of time flow. $|D(\text{real})-D(\text{gen})|$ goes down as training proceeds (upper row), and as $|D(\text{real})-D(\text{gen})|$ goes down, image quality goes up (lower row).

4.2.2 On the relation of discriminator outputs to image quality

As discussed in Section 2.2, successful training should make it harder and harder for the discriminator to distinguish real images and generated images, which would manifest as the discriminator output values for real images and generated images becoming closer and closer to each other. To see if this is actually the case, we looked into the discriminator output.

In Figure 10, we plot ‘ $|D(\text{real})-D(\text{gen})|$ ’, which is the absolute value of the difference between the discriminator output values for real images and those for generated images on average during training. The discriminator output values were obtained as a by-product of the forward propagation for updating the discriminator (i.e., in the U -minibatch update in ICFG). In Figure 10, the graphs in the upper row show $|D(\text{real})-D(\text{gen})|$ of xICFG in the log-scale (the y -axis), in relation to training runtime (the x -axis). The trend is the same on all the tested datasets. $|D(\text{real})-D(\text{gen})|$ of xICFG goes down as training proceeds, as expected. The graphs in the lower row plot the inception scores (the y -axis) in relation to $|D(\text{real})-D(\text{gen})|$ (the x -axis), where the arrows indicate the time flow. The trend is the same for all. With xICFG, improvement of image quality correlates with the decrease of $|D(\text{real})-D(\text{gen})|$, as suggested by the theory. This is in contrast to GAN, where the discriminator output values show little correlation to generator performance (see e.g., [1]).

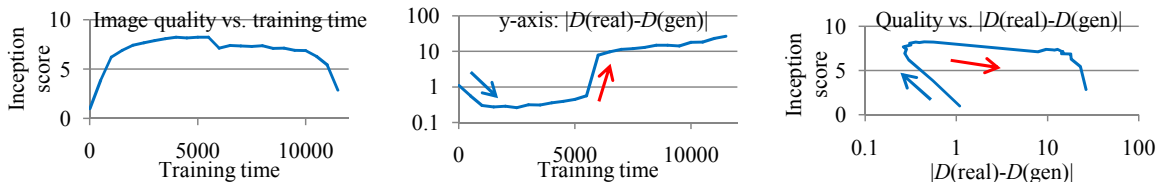


Figure 11: Example of generator degradation, artificially induced by a small training set (1000 examples). xICFG. $|D(\text{real})-D(\text{gen})|$ and the inception score show a good correlation. Thus, $|D(\text{real})-D(\text{gen})|$ serves as a good indicator of xICFG training progress.

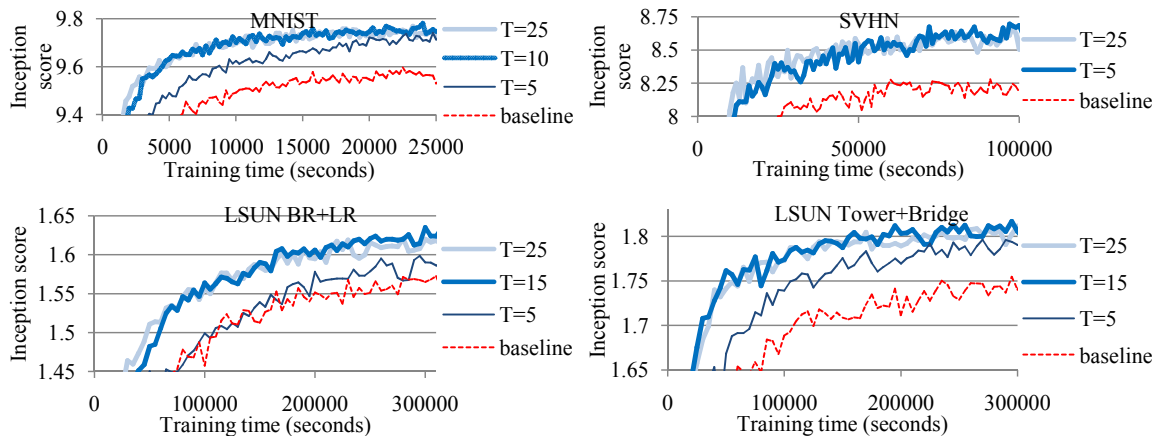


Figure 12: On the values for T (number of ICFG iterations, which determines the generator size). With convolutional approximators as in Figure 2. T can be reduced from 25 to 5 (SVHN), 10 (MNIST), or 15 (LSUN) without negative consequences. “baseline” is the best baseline performance copied from Figure 2.

In Figure 11, we show how $|D(\text{real}) - D(\text{gen})|$ changes in the case of training failure of xICFG, artificially induced by a small training set (1000 real data examples). In this example, soon after $|D(\text{real}) - D(\text{gen})|$ value starts going up, the inception score, indicative of the quality of generated images, plateaus and starts going down. In this particular scenario, the discriminator is overfitting to the small set of real data and causing the violation of the ϵ -approximation assumption of our theory. That slows down and eventually stops the progress of the generator, resulting in the increase of $|D(\text{real}) - D(\text{gen})|$. The behavior conforms to the theory.

Thus, one can use $|D(\text{real}) - D(\text{gen})|$ values, which can be obtained at almost no cost during training, as an indicator of the success/failure/progress of training of xICFG.

4.2.3 On the values for T (number of ICFG iterations)

To obtain the results presented so far, for simplicity, we fixed meta-parameters (except for step size η) to the values in Table 1 in all the settings across the datasets and the network architectures. In this section, we seek smaller values for T (the number of iterations in ICFG) to pursue practical advantages of small generators. Recall that an xICFG generator takes the form of G_T resulting from T iterations of $G_t(z) \leftarrow G_{t-1}(z) + \eta g_t(G_{t-1}(z))$, and the size of G_T depends on T as illustrated in Figure 1. While a sufficiently large T stabilizes training by ensuring that training makes progress by overcoming the degradation caused by approximation, a smaller T leads to a smaller generator resulting in faster generation and smaller footprints during both training and generation. The results presented so far were obtained by setting $T = 25$, which worked well for both strong (convolutional) and weak (fully-connected) approximators. We show in Figure 12 the results of testing several values for T with strong (convolutional) approximators used in Figure 2. We observe that setting $T=5$ (SVHN), 10 (MNIST), or 15 (LSUN) is as good as $T=25$; i.e., T can be reduced from 25 to the respective values to receive the advantages of a smaller T , without negative consequences. Reducing T further to 5 results in lower inception scores (except for SVHN), though still outperforming the best baseline method.

Use of the final approximator as a generator Since G_t for $t = 0, \dots, T-1$ can also serve as a generator, the generator size can be further reduced by using one of them at the expense of some quality degradation. In particular, the final approximator (used as G_0 in the final call of ICFG), is the smallest. In the table below, we show the inception scores of the final approximator in comparison with the final generator and the best baseline method. Here, training was done with T set to the values found to be good in Figure 12.

	MNIST $T=10$	SVHN $T=5$	LSUN BR+LR $T=15$	LSUN T+B $T=15$
Final generator (G_T)	9.79	8.68	1.64	1.81
Final approximator (G_0)	9.65	8.53	1.62	1.80
Best baseline	9.54	8.18	1.57	1.74

We observe that while the final approximator underperforms the final generator as expected, it is still better than the best baseline method, whose generator uses exactly the same network design (and therefore of the same size) as the final approximator. Thus, use of the final approximator as a generator is a viable option when faster generation and/or a smaller footprint of generation is required. The results also indicate that the higher performance (in terms of the inception score) of xICFG is attributed to not only having a larger (and therefore more complex) generator but also stable and efficient training, which makes it possible to refine the approximator network to the degree that it can outperform the baseline methods.

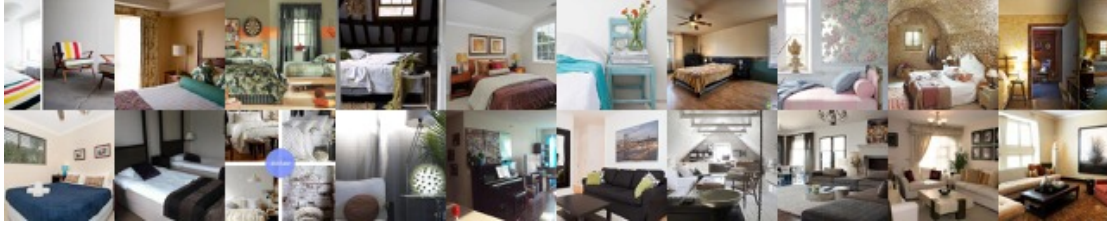
5 Conclusion

In the generative adversarial learning setting, we considered a generator that can be obtained using composite functional gradient learning. Our theoretical results led to the new stable algorithm xICFG. The experimental results showed that xICFG generated equally good or better images than GAN and WGAN variants in a stable manner on commonly used datasets.

Although this paper only studied the application of composite functional gradient learning (CFG) in the setting of generative adversarial models, it is clear that the general concept of CFG should be applicable to other problems. This will be a promising direction for future work.

References

- [1] Martin Arjovsky, Soumith Chintala, and Léon Bottou. Wasserstein generative adversarial networks. In *International Conference on Machine Learning (ICML)*, 2017.
- [2] Jimmy Lei Ba, Jamie Ryan Kiros, and Geoffrey E. Hinton. Layer normalization. *arXiv:1607.06450*, 2016.
- [3] David Berthelot, Thomas Schumm, and Luke Metz. BEGAN: Boundary equilibrium generative adversarial networks. *arXiv:1703.10717*, 2017.
- [4] Tong Che, Yanran Li, Athul Paul Jacob, Yoshua Bengio, and Wenjie Li. Mode regularized generative adversarial networks. In *Proceedings of International Conference on Learning Representations (ICLR)*, 2017.
- [5] Jerome H. Friedman. Greedy function approximation: a gradient boosting machine. *Ann. Statist.*, 29(5):1189–1232, 2001.
- [6] Ian J. Goodfellow, Jean Pouget-Abadie, Mehdi Mirza, Bing Xu, David Warde-Farley, Shejil Ozair, Aaron Courville, and Yoshua Bengio. Generative adversarial nets. In *NIPS*, 2014.
- [7] Ishaan Gulrajani, Faruk Ahmed, Martin Arjovsky, Vincent Dumoulin, and Aaron Courville. Improved training of Wasserstein GANs. In *Advances in Neural Information Processing Systems 30 (NIPS 2017)*, 2017.
- [8] Kaiming He, Xiangyu Zhang, Shaoqing Ren, and Jian Sun. Deep residual learning for image recognition. *arXiv:1512.03385*, 2015.
- [9] Diederik P. Kingma and Jimmy Ba. Adam: A method for stochastic optimization. In *Proceedings of International Conference on Learning Representations (ICLR)*, 2015.



(a) Real images in the training set.



(b) Generated by xICFG with 4-block ResNets.



(c) Generated by the best baseline method (WGANgp) with 4-block ResNets.

Figure 13: LSUN bedrooms & living rooms.



(a) Real images in the training set.



(b) Generated by xICFG with 4-block ResNets.



(c) Generated by the best baseline method (WGANgp) with 4-block ResNets.

Figure 14: LSUN towers & bridges.

- [10] Justin Lazarow, Long Jin, and Zhuowen Tu. Introspective neural networks for generative modeling. In *Proceedings of International Conference on Computer Vision (ICCV)*, 2017.
- [11] Xudong Mao, Qing Li, Haoran Xie, Raymond Y.K. Lau, Zhen Wang, and Stephen Paul Smolley. Least squares generative adversarial networks. *arXiv:1611.04076*, 2017.
- [12] Luke Metz, Ben Poole, David Pfau, and Jascha Sohl-Dickstein. Unrolled generative adversarial networks. In *Proceedings of International Conference on Learning Representations (ICLR)*, 2017.
- [13] Youssef Mroueh and Tom Sercu. Fisher GAN. In *Advances in Neural Information Processing Systems 30 (NIPS 2017)*, 2017.
- [14] Yuval Netzer, Tao Wang, Adam Coates, Alessandro Bissacco, Bo Wu, and Andrew Y. Ng. Reading digits in natural images with unsupervised feature learning. In *Proceedings of NIPS Workshop on Deep Learning and Unsupervised Feature Learning*, 2011.
- [15] Alec Radford, Luke Metz, and Soumith Chintala. Unsupervised representation learning with deep convolutional generative adversarial networks. *arXiv:1511.06434*, 2015.
- [16] Tim Salimans, Ian Goodfellow, Wojciech Zaremba, Vicki Cheung, Alec Radford, and Xi Chen. Improved techniques for training GANs. In *Advances in Neural Information Processing Systems 29 (NIPS 2016)*, 2016.
- [17] Lucas Theis, Aäron van den Oord, and Matthias Bethge. A note on the evaluation of generative models. In *Proceedings of International Conference on Learning Representations (ICLR)*, 2016.
- [18] Tijman Tieleman and Geoffrey Hinton. Lecture 6.5-rmsprop: Divide the gradient by a running average of its recent magnitude. *COURSERA: Neural Networks for Machine Learning*, 4, 2012.
- [19] Ilya Tolstikhin, Sylvain Gelly, Olivier Bousquet, Carl-Johann Simon-Gabriel, and Bernhard Schölkopf. AdaGAN: Boosting generative models. In *Advances in Neural Information Processing Systems 30 (NIPS 2017)*, 2017.
- [20] David Warde-Farley and Yoshua Bengio. Improving generative adversarial networks with denoising feature matching. In *Proceedings of International Conference on Learning Representations (ICLR)*, 2017.
- [21] Jianwei Yang, Anitha Kannan, Dhruv Batra, and Devi Parikh. LR-GAN: Layered recursive generative adversarial networks for image generation. In *Proceedings of International Conference on Learning Representations (ICLR)*, 2017.

A Proof of Theorem 2.1

Given a differentiable scalar function $h(x) : \mathbb{R}^r \rightarrow \mathbb{R}$, we use $\nabla h(x)$ to denote its gradient, which becomes a r -dimensional vector function. Given a differentiable function $g(x) : \mathbb{R}^r \rightarrow \mathbb{R}^r$, we use $\nabla g(x)$ to denote its Jacobi matrix and we use $\nabla \cdot g(x)$ to denote the divergence of $g(x)$, defined as

$$\nabla \cdot g(x) := \sum_{j=1}^r \frac{\partial g(x)}{\partial [x]_j},$$

where we use $[x]_j$ to denote the j -th component of x . We know that

$$\int \nabla \cdot w(x) dx = 0 \quad (8)$$

for all vector function $w(x)$ such that $w(\infty) = 0$.

Lemma A.1 *Assume that $g(x) : \mathbb{R}^r \rightarrow \mathbb{R}^r$ is a continuously differentiable transformation. Assume that $\|g(x)\| \leq a$ and $\|\nabla g(x)\| \leq b$, then as $\eta b < 1$, the inverse transformation $x = f^{-1}(x')$ of $x' = f(x) = x + \eta g(x)$ is unique.*

Moreover, consider transformation of random variables by $f^{-1}(\cdot)$. Define \tilde{p}_ to be the associated probability density function after this transformation when the pdf before the transformation is p_* . Then for any $x \in \mathbb{R}^r$, we have:*

$$\tilde{p}_*(x) = p_*(f(x)) |\det(\nabla f(x))|. \quad (9)$$

Similarly, we have

$$p(x) = p'(f(x)) |\det(\nabla f(x))|, \quad (10)$$

where p and p' are defined in Theorem 2.1.

Proof Given x' , define map $g'(x)$ as $g'(x) = x' - \eta g(x)$, then the assumption implies that $g'(x)$ is a contraction when $\eta b < 1$: $\|g'(x) - g'(x')\| \leq \eta b \|x - x'\|$. Therefore $g'(x)$ has a unique fixed point x , which leads to the inverse transformation $f^{-1}(x') = x$.

(9) and (10) follow from the standard density formula under transformation of variables. ■

Lemma A.2 *Under the assumptions of Lemma A.1, there exists a constant $c > 0$ such that*

$$|\det(\nabla f(x)) - (1 + \eta \nabla \cdot g(x))| \leq c\eta^2. \quad (11)$$

Proof

We note that

$$\nabla f(x) = I + \eta \nabla g(x).$$

Therefore

$$\det(\nabla f(x)) = 1 + \eta \nabla \cdot g(x) + \sum_{j \geq 2} \eta^j m_j(g(x)),$$

where $m_j(g)$ is a function of ∇g . Since ∇g is bounded, we obtain the desired formula. ■

Lemma A.3 *Under the assumptions of Lemma A.1, and assume that Assumption 2.1 holds, then there exists a constant $c > 0$ such that*

$$\int |\tilde{p}_*(x) - (p_*(x) + \eta p_*(x) \nabla \cdot g(x) + \eta \nabla p_*(x)^\top g(x))| dx \leq c\eta^2. \quad (12)$$

and

$$\int \frac{(\tilde{p}_*(x) - p_*(x))^2}{p_*(x)} dx \leq c\eta^2. \quad (13)$$

Proof Using the algebraic inequality

$$\begin{aligned}
& |p_*(f(x))| \det(\nabla f(x)) - (p_*(x) + \eta p_*(x) \nabla \cdot g(x) + \eta \nabla p_*(x)^\top g(x))| \\
& \leq |p_*(f(x)) - (p_*(x) + \eta \nabla p_*(x)^\top g(x))| |\det(\nabla f(x))| \\
& \quad + |(p_*(x) + \eta \nabla p_*(x)^\top g(x))| |(1 + \eta \nabla \cdot g(x)) - |\det(\nabla f(x))|| \\
& \quad + \eta^2 |\nabla \cdot g(x) \nabla p_*(x)^\top g(x)|,
\end{aligned}$$

and using $\tilde{p}_*(x) = p_*(f(x)) |\det(\nabla f(x))|$ from (9), we obtain

$$\begin{aligned}
& \int |\tilde{p}_*(x) - (p_*(x) + \eta p_*(x) \nabla \cdot g(x) + \eta \nabla p_*(x)^\top g(x))| dx \\
& \leq \underbrace{\int |p_*(f(x)) - (p_*(x) + \eta \nabla p_*(x)^\top g(x))| |\det(\nabla f(x))| dx}_{A_0} \\
& \quad + \underbrace{\int |(p_*(x) + \eta \nabla p_*(x)^\top g(x))| |(1 + \eta \nabla \cdot g(x)) - |\det(\nabla f(x))|| dx}_{B_0} \\
& \quad + \eta^2 \underbrace{\int |\nabla \cdot g(x) \nabla p_*(x)^\top g(x)| dx}_{C_0} \\
& \leq c\eta^2
\end{aligned}$$

for some constant $c > 0$, which proves (12). The last inequality uses the following facts.

$$A_0 = \int |p_*(f(x)) - (p_*(x) + \eta \nabla p_*(x)^\top g(x))| O(1) dx = O(\eta^2),$$

where the first equality follows from the boundedness of g and ∇g , and the second equality follows from the first inequality of Assumption 2.1.

$$B_0 = \int |(p_*(x) + \eta \nabla p_*(x)^\top g(x))| O(\eta^2) dx = O(\eta^2),$$

where the first equality follows from (11), and the second equality follows from the third equality of Assumption 2.1.

$$C_0 = \int \|\nabla p_*(x)\| O(1) dx = O(1),$$

where the first equality follows from the boundedness of g and ∇g , and the second equality follows from the third equality of Assumption 2.1.

Moreover, using (9), we obtain

$$|\tilde{p}_*(x) - p_*(x)| \leq |p_*(f(x)) - p_*(x)| |\det(\nabla f(x))| + p_*(x) |\det(\nabla f(x))| - 1|.$$

Therefore

$$\begin{aligned}
& \int \frac{(\tilde{p}_*(x) - p_*(x))^2}{p_*(x)} dx \\
& \leq 2 \int \frac{(p_*(f(x)) - p_*(x))^2 |\det(\nabla f(x))|^2 + p_*(x)^2 (|\det(\nabla f(x))| - 1)^2}{p_*(x)} dx \leq c\eta^2
\end{aligned}$$

for some $c > 0$, which proves (13). The second inequality follows from the second inequality of Assumption 2.1, and the boundedness of $|\det(\nabla f(x))|$, and the fact that $||\det(\nabla f(x))| - 1| = O(\eta)$ from (11). \blacksquare

Proof of Theorem 2.1

In the following integration, with a change of variable from x to x' using $x' = f(x)$ as in Lemma A.1, we obtain

$$\begin{aligned}
& \int (\beta p_*(x') + (1 - \beta)p'(x')) \ln \frac{\beta p_*(x') + (1 - \beta)p'(x')}{(1 - \beta)p_*(x') + \beta p'(x')} dx' \\
&= \int (\beta p_*(f(x)) + (1 - \beta)p'(f(x))) \ln \frac{\beta p_*(f(x)) + (1 - \beta)p'(f(x))}{(1 - \beta)p_*(f(x)) + \beta p'(f(x))} |\det(\nabla f(x))| dx \\
&= \int (\beta \tilde{p}_*(x) + (1 - \beta)p(x)) \ln \frac{\beta \tilde{p}_*(x) + (1 - \beta)p(x)}{(1 - \beta)\tilde{p}_*(x) + \beta p(x)} dx,
\end{aligned}$$

where the first inequality is basic calculus, and the second inequality uses (9) and (10).

It follows that

$$\begin{aligned}
L_\beta(p') &= \int (\beta p_*(x') + (1 - \beta)p'(x')) \ln \frac{\beta p_*(x') + (1 - \beta)p'(x')}{(1 - \beta)p_*(x') + \beta p'(x')} dx' \\
&= \int (\beta \tilde{p}_*(x) + (1 - \beta)p(x)) \ln \frac{\beta \tilde{p}_*(x) + (1 - \beta)p(x)}{(1 - \beta)\tilde{p}_*(x) + \beta p(x)} dx \\
&= A_1 + B_1 + C_1,
\end{aligned}$$

where A_1 , B_1 , and C_1 are defined as follows.

$$\begin{aligned}
A_1 &= \int (\beta \tilde{p}_*(x) + (1 - \beta)p(x)) \ln \frac{\beta p_*(x) + (1 - \beta)p(x)}{(1 - \beta)p_*(x) + \beta p(x)} dx \\
&= \int (\beta p_*(x) + (1 - \beta)p(x)) \ln \frac{\beta p_*(x) + (1 - \beta)p(x)}{(1 - \beta)p_*(x) + \beta p(x)} dx \\
&\quad + \eta\beta \int (p_*(x)\nabla \cdot g(x) + \nabla p_*(x)^\top g(x)) \ln \frac{\beta p_*(x) + (1 - \beta)p(x)}{(1 - \beta)p_*(x) + \beta p(x)} dx + O(\eta^2) \\
&= L_\beta(p) + \beta\eta \int \nabla \cdot (p_*(x)g(x)) \mathcal{D}(x) dx + O(\eta^2) \\
&= L_\beta(p) + \beta\eta \int \nabla \cdot (p_*(x)g(x)) D_\epsilon(x) dx + O(\eta\epsilon + \eta^2) \\
&= L_\beta(p) - \beta\eta \int p_*(x)g(x)^\top \nabla D_\epsilon(x) dx + O(\eta\epsilon + \eta^2),
\end{aligned}$$

where the second equality uses (12) and the fact that $B < \infty$ in the statement of the theorem. The fourth equality uses the ϵ -approximation condition of the theorem statement. The last equality uses integration by parts and (8).

$$\begin{aligned}
B_1 &= \int (\beta \tilde{p}_*(x) + (1 - \beta)p(x)) \ln \frac{\beta \tilde{p}_*(x) + (1 - \beta)p(x)}{\beta p_*(x) + (1 - \beta)p(x)} dx \\
&= \int (\beta \tilde{p}_*(x) + (1 - \beta)p(x)) \ln \left(1 + \beta \frac{\tilde{p}_*(x) - p_*(x)}{\beta p_*(x) + (1 - \beta)p(x)} \right) dx \\
&\leq \beta \int (\beta \tilde{p}_*(x) + (1 - \beta)p(x)) \frac{\tilde{p}_*(x) - p_*(x)}{\beta p_*(x) + (1 - \beta)p(x)} dx \\
&= \beta^2 \int \frac{(\tilde{p}_*(x) - p_*(x))^2}{\beta p_*(x) + (1 - \beta)p(x)} dx = O(\eta^2),
\end{aligned}$$

where the inequality uses $\ln(1 + \delta) \leq \delta$. The last equality uses (13).

$$\begin{aligned}
C_1 &= \int (\beta \tilde{p}_*(x) + (1 - \beta)p(x)) \ln \frac{(1 - \beta)p_*(x) + \beta p(x)}{(1 - \beta)\tilde{p}_*(x) + \beta p(x)} dx \\
&= \int (\beta \tilde{p}_*(x) + (1 - \beta)p(x)) \ln \left(1 + (1 - \beta) \frac{p_*(x) - \tilde{p}_*(x)}{(1 - \beta)\tilde{p}_*(x) + \beta p(x)} \right) dx \\
&\leq (1 - \beta) \int (\beta \tilde{p}_*(x) + (1 - \beta)p(x)) \frac{p_*(x) - \tilde{p}_*(x)}{(1 - \beta)\tilde{p}_*(x) + \beta p(x)} dx \\
&= (1 - \beta) \int (\beta \tilde{p}_*(x) + (1 - \beta)p(x)) \frac{p_*(x) - \tilde{p}_*(x)}{(1 - \beta)p_*(x) + \beta p(x)} dx \\
&\quad + (1 - \beta)^2 \int (\beta \tilde{p}_*(x) + (1 - \beta)p(x)) \frac{(p_*(x) - \tilde{p}_*(x))^2}{((1 - \beta)\tilde{p}_*(x) + \beta p(x))((1 - \beta)p_*(x) + \beta p(x))} dx \\
&\stackrel{(a)}{=} (1 - \beta) \int (\beta \tilde{p}_*(x) + (1 - \beta)p(x)) \frac{p_*(x) - \tilde{p}_*(x)}{(1 - \beta)p_*(x) + \beta p(x)} dx + O(\eta^2) \\
&\stackrel{(b)}{=} - (1 - \beta) \int (\beta p_*(x) + (1 - \beta)p(x)) \frac{\eta p_*(x) \nabla \cdot g(x) + \eta \nabla p_*(x)^\top g(x)}{(1 - \beta)p_*(x) + \beta p(x)} dx + O(\eta^2) \\
&= - (1 - \beta) \eta \int (p_*(x) \nabla \cdot g(x) + \nabla p_*(x)^\top g(x)) \exp(\mathcal{D}(x)) dx + O(\eta^2) \\
&\stackrel{(c)}{=} - (1 - \beta) \eta \int (p_*(x) \nabla \cdot g(x) + \nabla p_*(x)^\top g(x)) \exp(D_\epsilon(x)) dx + O(\eta\epsilon + \eta^2) \\
&= - (1 - \beta) \eta \int (\nabla \cdot (p_*(x)g(x))) \exp(D_\epsilon(x)) dx + O(\eta\epsilon + \eta^2) \\
&= \eta(1 - \beta) \int p_*(x)g(x)^\top \nabla \exp(D_\epsilon(x)) dx + O(\eta\epsilon + \eta^2),
\end{aligned}$$

where the first inequality uses $\ln(1 + \delta) \leq \delta$. The equality (a) uses (13). The equality (b) uses (12). The equality (c) uses the ϵ -approximation condition of $D_\epsilon(x)$. The last equality uses integration by parts and (8).

By combining the estimates of A_1 , B_1 , and C_1 , we obtain the desired bound.

B Network architectures

The network definitions below include batch normalization layers. Note that to experiment with WGANgp, we explored the options with the batch normalization layers being removed or replaced, as described in Section 4.1.4.

B.1 MNIST and SVHN in Figure 2

The convolutional architectures used for MNIST and SVHN are an extension of DCGAN, inserting 1×1 convolution layers.

Approximator/Generator		Discriminator	
1	Projection	1	Convolution, 5×5 , stride 2
2	ReLU	2	LeakyReLU
3	Transposed conv, 5×5 , stride 2	3	Convolution, 5×5 , stride 2
4	BatchNorm	4	BatchNorm
5	ReLU	5	LeakyReLU
6	Convolution, 1×1 , stride 1	6	Convolution, 1×1 , stride 1
7	BatchNorm	7	BatchNorm
8	ReLU	8	LeakyReLU
9	Transposed conv, 5×5 , stride 2	9	Flatten
10	tanh	10	Linear

Repeat 2–7 twice. Repeat 3–8 twice.

For the discriminator, start with 32 (MNIST) or 64 (SVHN) feature maps and double it at downsampling except for the first downsampling. For the approximator/generator, start with 128 (MNIST) or 256 (SVHN) and halve it at upsampling except for the last upsampling.

B.2 LSUN in Figure 2

The convolutional architecture used for LSUN was adopted from https://github.com/igul222/improved_wgan_training. Both the approximator/generator and discriminator are a ResNet with four convolution blocks.

Approximator/Generator		Discriminator	
1	Project	1	Convolution, 3×3 , stride 1
2	BatchNorm	2	ReLU
3	ReLU	3	Convolution, 3×3 , stride 1
4	Upsampling ($\times 2$), nearest	4	Downsampling ($/2$), mean
5	Convolution, 3×3 , stride 1	5	BatchNorm
6	BatchNorm	6	ReLU
7	ReLU	7	Convolution, 3×3 , stride 1
8	Convolution, 3×3 , stride 1	8	BatchNorm
9	BatchNorm	9	ReLU
10	ReLU	10	Convolution, 3×3 , stride 1
11	Convolution, 3×3 , stride 1	11	Downsampling ($/2$), mean
12	tanh	12	ReLU

Repeat 2–9 four times. Repeat 5–11 three times.

2–9 of the approximator/generator and 1–4 and 5–12 of the discriminator are convolution blocks with a shortcut from the beginning to the end. The numbers of feature maps of the convolution layers are 512, 256, 256, 128, 128, 64, 64, and 64 for the approximator/generator, and 64, 64, 64, 128, 128, 256, 256, and 512 for the discriminator.